Cite this: *Nanoscale*, 2020, **12**, 3958

Spin curvature induced resistivity in epitaxial half-metallic CrO₂ thin films

Lijuan Qian,  Wenzhe Chen and Gang Xiao *

Spin configuration inside a ferromagnetic metal influences its magnetoresistive behavior. The local spin curvature induces excess resistivity from the homogeneous ferromagnetic state. In this work, we characterize the spin curvature induced resistivity in epitaxial half-metallic CrO₂ nanowires with 100% spin polarization. We control the magnitude of the spin curvature by introducing different geometric notches along the edge of the wire and applying an external magnetic field. Through magnetoresistance measurements and micromagnetic simulations, we uncover an empirical relationship between the spin curvature and the induced resistivity in this archetypal half-metallic solid. This relationship provides a quantitative method to calculate the resistance of magnetic domain walls or other spin textured states. We also study the influence of the thermal effect on the spin curvature induced resistivity across temperatures ranging from 10 K to 250 K. Thermal magnons worsen spin asymmetry considerably and suppress spin curvature induced resistivity at temperatures much lower than the ferromagnetic ordering temperature T_c .

Received 5th November 2019,

Accepted 4th January 2020

DOI: 10.1039/c9nr09443a

rsc.li/nanoscale

Introduction

Spin dependent electron transport has been observed in various physical systems such as the anomalous Hall effect,^{1,2} spin Hall effect,^{3–9} and domain wall resistance.^{10–14} In ferromagnetic metals, the resistivity is strongly affected by detailed spin configurations due to their spin dependent electronic structures and magneto-transport.^{15–22} For example, magnetic domain wall resistivity (DWR) represents an excess resistivity resulting from the non-uniformity of spins within a single domain wall.^{12,13,17} In this work, we quantify the spatial non-uniformity of spins as the spin curvature. According to Levy and Zhang's model of DWR based on the two-spin-current-channel theory, the essential element inducing excess resistivity is the spin curvature.¹⁷ Spin curvature not only exists in a domain wall but can also be induced and manipulated through sample geometry and external field, and is the essential element of different spin textures.^{14,23,24} Understanding the effect of spin curvature on electron transport is fundamentally important for innovative magnetic logic²⁵ and memory¹⁰ device applications. One of the best materials for this type of study is a half-metallic ferromagnet with 100% spin polarization.^{26,27} Due to its strongly spin dependent electronic structure, it is expected that the presence of spin curvature would induce a large excess of resistivity in half metals. CrO₂ was first predicted to be a half metal by Schwarz in 1986²⁸ and confirmed

as such through various experimental techniques^{29–31} and by detailed band structure calculations.^{32,33}

In this work, we characterize spin curvature induced resistivity in epitaxial CrO₂ nanowires by intentionally creating geometrical objects: notches, along the edge of a nanowire. We have observed a positive correlation between the magnetoresistance (MR) and the spin curvature. In the moderate field range ($|B| < 0.2$ T), MR depends on the spin curvature linearly. We have also studied the effect of temperature on the MR and spin curvature in the temperature range of 10 to 250 K, below the Curie temperature ($T_c \approx 390$ K).³⁴ The amplitude of the MR and the dependence of the MR on the spin curvature decrease with increasing temperature because of reduced spin asymmetry.

Experiments and characterization

We fabricated epitaxial CrO₂ nanowires without post-deposition patterning using chemical vapor deposition (CVD) and selective area growth.^{35,36} First, we deposited a 100 nm-thick SiO₂ film using magnetron sputtering on an insulating TiO₂ substrate, which has the same rutile crystal structure as CrO₂ and similar lattice constants to it. We then spin-coated a 200 nm-thick electron beam resist layer (950 PMMA A4) onto the sample, followed by the deposition of a 5 nm-thick conducting Cr layer. Using electron-beam lithography and reactive ion etching with CHF₃ (removing SiO₂), we exposed the TiO₂ substrate in the form of a nanowire as shown in Fig. 1(a). Finally, using CVD, we deposited a 100 nm-thick CrO₂ nano-

Department of Physics, Brown University, Providence, RI 02912, USA.

E-mail: gang_xiao@brown.edu

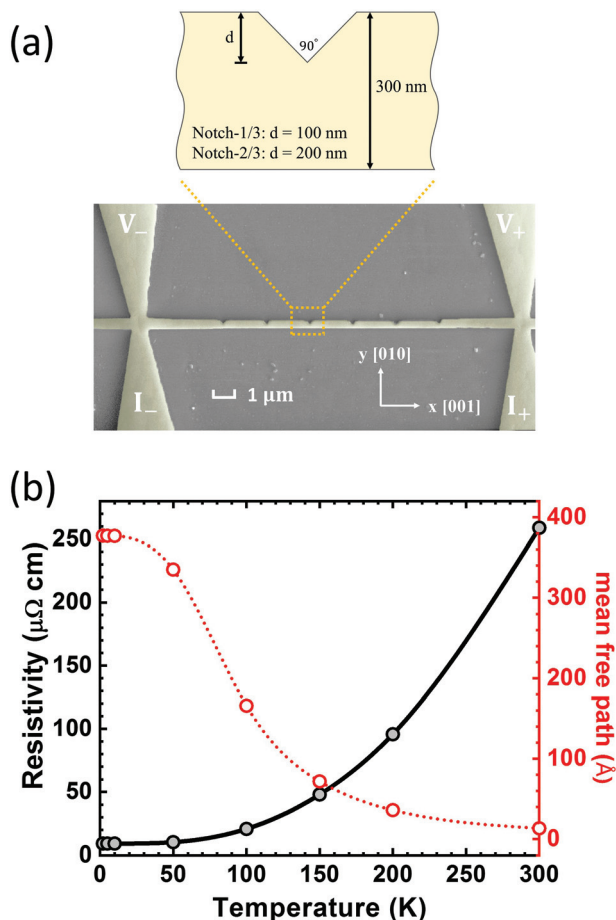


Fig. 1 (a) Schematic and SEM image of a typical sample. Each sample is a 300 nm-width wire with 6 notches. The four leads are designed for 4-wire transport measurements. The samples are classified as Notch-1/3 and Notch-2/3 according to the notch depth in the schematic. (b) The resistivity and estimated mean free path of the Notch-1/3 sample in the temperature range from 2 to 300 K.

wire directly onto the TiO_2 substrate without the requirement of post-deposition patterning, which tends to generate edge and surface defects in a nanowire. The method of selective area growth is made possible because the sticking coefficient of CrO_2 vapor on SiO_2 is null. Previous studies²⁹ have determined that the spin polarization is 0.96 ± 0.01 at 1.85 K in a CrO_2 thin film deposited with this method.

Fig. 1(a) shows the scanning electron micrograph (SEM) of a representative sample. The CrO_2 nanowire is along the easy axis [001] direction with a width w of 300 nm. There are six 90° notches localized along one edge of a nanowire to introduce spin curvature. We denote the two samples with the notch depth d of 100 nm and 200 nm as “Notch-1/3” and “Notch-2/3”, meaning “Notch- d/w ”, respectively. The nanowire has four leads for transport measurement. No grain boundaries are observed in the SEM, which confirms that the nanowires are epitaxial.

Fig. 1(b) shows the resistivity of the Notch-1/3 sample within the temperature range of 2 to 300 K. At 2 K, $\rho(2 \text{ K}) \approx$

$9.2 \mu\Omega \text{ cm}$, and at 300 K, $\rho(300 \text{ K}) \approx 259 \mu\Omega \text{ cm}$, with a residue resistivity ratio, $\text{RRR} = \rho(300 \text{ K})/\rho(2 \text{ K})$, of 28.2. These values are well comparable to those obtained for single crystal CrO_2 :³² $\rho(0 \text{ K}) \approx 5 \mu\Omega \text{ cm}$, $\rho(300 \text{ K}) \approx 250 \mu\Omega \text{ cm}$, and $\text{RRR} = 50$. We can estimate the electron mean free path using the approximate relation based on the Boltzmann theory,^{32,37}

$$l \cong \frac{(2\pi)^3 \hbar}{e^2} \frac{1}{A_{\text{FS}}^{\uparrow} + A_{\text{FS}}^{\downarrow}} \frac{3}{\bar{\rho}} \quad (1)$$

where $\bar{\rho}$ is the resistivity, and A_{FS}^{\uparrow} and $A_{\text{FS}}^{\downarrow}$ are the areas of the Fermi surfaces for the majority and minority electrons, respectively (for CrO_2 , $A_{\text{FS}}^{\uparrow} \approx 8.86 \text{ \AA}^{-2}$ and $A_{\text{FS}}^{\downarrow} \approx 0$).³² Based on the resistivity data given in Fig. 1(b), we determined that $l(2 \text{ K}) \approx 377 \text{ \AA}$ and $l(300 \text{ K}) \approx 13.3 \text{ \AA}$. These numbers are also close to the single crystal values of $l(0 \text{ K}) \approx 700 \text{ \AA}$ and $l(300 \text{ K}) \approx 14 \text{ \AA}$.³² Our analysis validates the high crystalline quality of our nanowire. The electron mean free path is much smaller than the dimension of the nanowire. Therefore, electron transport is diffusive rather than ballistic.

Results and discussion

We study the dependence of resistivity on the spin curvature by measuring the MR of our nanowire samples. Fig. 2(a) and (b) show the hysteresis loops of the MR ratio, defined as $\Delta R/R = [R(B) - R(0)]/R(0)$, for the Notch-1/3 sample at 10 K over a medium ($\pm 0.2 \text{ T}$) and a large ($\pm 6 \text{ T}$) magnetic field range, respectively. The initial magnetic field B is along the length of the wire, *i.e.*, the easy axis, as shown in Fig. 1(a). The same measurement is performed on the Notch-2/3 sample over a medium ($\pm 0.1 \text{ T}$) magnetic field range. In Fig. 2(a), as we increase the field from -0.2 T to 0 (point d) and then to $+0.02 \text{ T}$ (point e), the MR increases linearly from -0.182% to $+0.037\%$ with the field, followed by a sudden decrease in the MR from $+0.037\%$ (point e) to -0.033% (point f). Further increase in the field causes the MR to decrease linearly to -0.190% at $+0.2 \text{ T}$ (point g). In higher fields as shown in Fig. 2(b), the MR continues to decrease with the field and reach the minimum of -0.67% at $+2.0 \text{ T}$ (point h). Beyond $+2.0 \text{ T}$, the MR starts to increase with the field parabolically due to the strong Lorentz force on the electron motion.

To understand the MR behavior, we simulated spin maps for the Notch-1/3 sample in Fig. 2(d) to (h) in key magnetic fields, indices (d) to (h) correspond to points d to h as shown in Fig. 2(a) and (b). The simulation was carried out using Mumax^{38,39} software, based on the uniaxial anisotropy constant $K_u = 9.2 \times 10^4 \text{ erg cm}^{-3}$ for the 100 nm thick CrO_2 film,³⁴ the saturation magnetization $M_s = 640 \text{ emu cm}^{-3}$ for CrO_2 at 10 K,³⁴ and the exchange stiffness constant $A_{\text{ex}} = 4.6 \times 10^{-7} \text{ erg cm}^{-1}$ estimated from the Curie temperature.³⁴ To reduce the computational time, we simulate one notch with the length of $5 \mu\text{m}$, which is long enough to eliminate the effect of the edge on the magnetization near the notches. We confirmed the val-

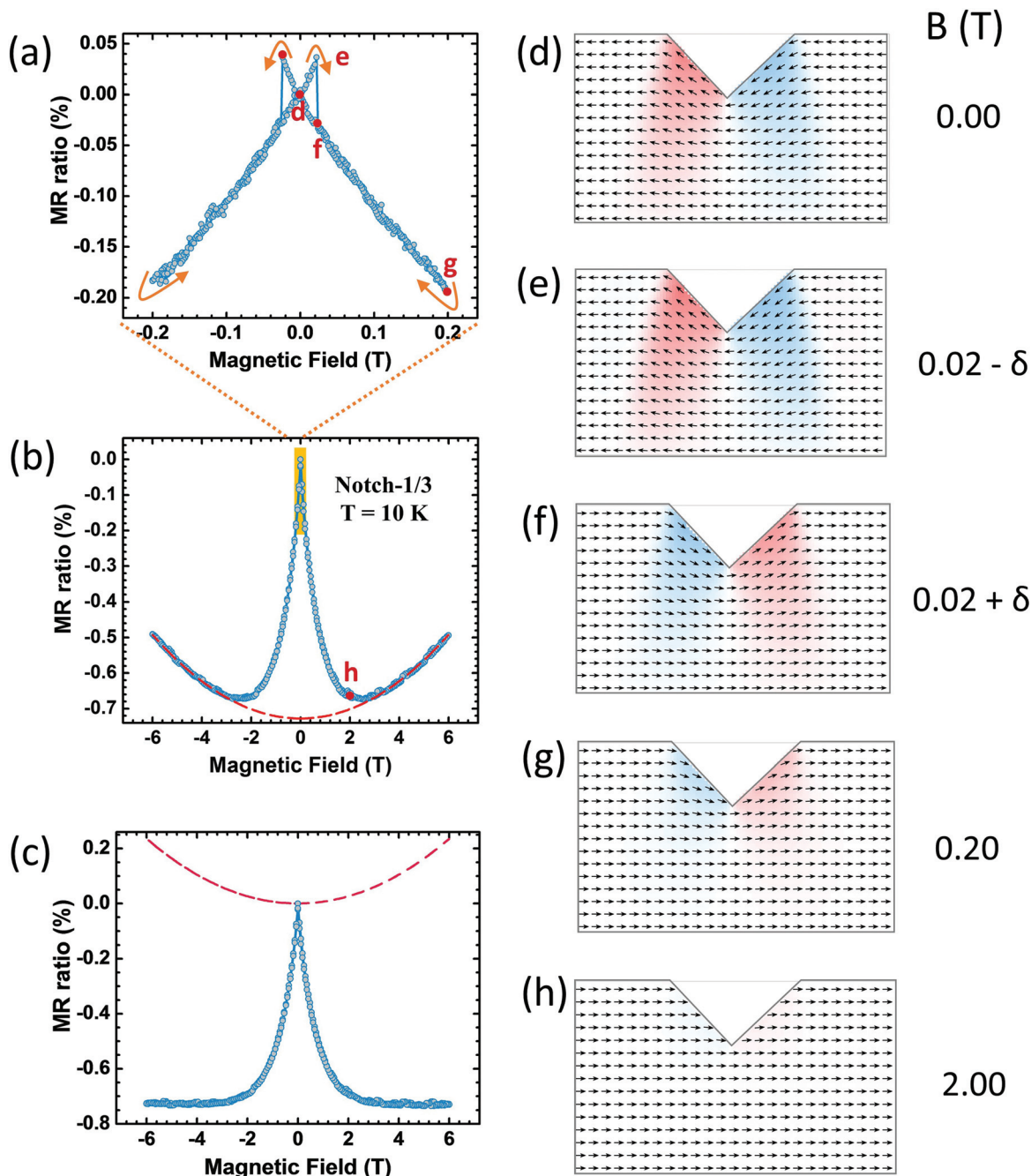


Fig. 2 (a) and (b) The magnetoresistance of the Notch-1/3 sample at 10 K within the field range of ± 0.2 T and ± 6 T. (c) The spin curvature induced magnetoresistance (blue) and the fitted Lorentz magnetoresistance (the red dashed line). (d)–(h) Simulated micromagnetic spin maps of the Notch-1/3 sample at magnetic fields corresponding to the states in (a) and (b) (points d–h).

idity of such approximation by performing a simulation with the exact same geometry as shown in Fig. 1(a), which shows the same spin map near the notches. In Fig. 2(d) to (h), the color scale represents the y component of \vec{M} (blue along $-y$ and red along $+y$). The spin map is the result of the competition among multiple energy components,

$$E = E_{\text{magnetostatic}} + E_{\text{Zeeman}} + E_{\text{exchange}} + E_{\text{anisotropy}} \quad (2)$$

The shape anisotropy energy $E_{\text{magnetostatic}}$ is determined by the sample geometrical details and has the tendency to align the spins near the edges to be parallel along the edges. $E_{\text{magnetostatic}}$ is the main culprit behind the local spin curvature near the notches. The magnetocrystalline anisotropy energy $E_{\text{anisotropy}}$ defines the easy axis along the length of the nanowire. The Zeeman energy $E_{\text{Zeeman}} = -\mu_0 \int \vec{M} \cdot \vec{B} dV$ forces the spins to the direction of the external field. The exchange

energy E_{exchange} is responsible for the ferromagnetic ordering.

We simulate the spin maps in the following sequence. Starting at $B = -0.20$ T, we gradually bring the field to zero (point d), and the corresponding spin map is shown in Fig. 2(d). The overall \vec{M} vector is along the $-x$ direction. Increasing B to $+(0.02 - \delta)$ T (point e) introduces more spin curvature in the spin map as shown in Fig. 2(e) in order to lower the Zeeman energy. At this moment, a slight increase in B to $+(0.02 + \delta)$ T (point f) leads to a switching of \vec{M} to the $+x$ direction as well as a sudden decrease in the spin curvature due to the sign reversal of the Zeeman energy. Fig. 2(f) shows the corresponding spin map. The sudden decrease in the MR in Fig. 2(a) is caused by such a decrease in the spin curvature. B increases to $+0.20$ T at point g, and the corresponding spin map is shown in Fig. 2(g), where it becomes obvious that all the spins tend to be aligned along the $+x$ direction with reduced spin curvature. When B is as large as 2.0 T, all the spins align perfectly along the $+x$ direction as shown in Fig. 2(h) and the MR value saturates to its minimum without the spin curvature.

A simulated spin map reveals the spin curvature in the corresponding field. For further analysis of the spin curvature dependent MR, we must exclude the contribution from other MR effects such as anisotropic magnetoresistance (AMR) and Lorentz MR. The AMR contribution is due to the angular variation between the electrical current density and the local magnetization vector,^{15,40} as described by the following relation:

$$\rho(\theta) = \rho_{\perp} + (\rho_{\parallel} - \rho_{\perp})\cos^2 \theta \quad (3)$$

where θ is the angle between the magnetization (\vec{M}) and the current flow direction (\vec{j}), i.e., $\cos \theta = \frac{\vec{j} \cdot \vec{M}}{|\vec{j}| |\vec{M}|}$; ρ_{\perp} and ρ_{\parallel} are the resistivities when \vec{j} is perpendicular and parallel to \vec{M} , respectively. Anwar *et al.* have found $\frac{\rho_{\parallel} - \rho_{\perp}}{\rho_0} = 0.7\%$ in epitaxial CrO₂ thin films at 4.2 K.⁴¹ From the simulated spin maps $\vec{M}(x, y)$ as shown in Fig. 2(d)–(h) and the current flow map $\vec{j}(x, y)$, which is calculated from the same notch geometry using COMSOL Multiphysics®, we derive a distribution of resistivity $\rho(x, y)$ using eqn (3) in different fields. By feeding the distribution of resistivity $\rho(x, y)$ into COMSOL Multiphysics®, we derive the resistance in the corresponding fields under AMR. The resistance difference at 0 T and 2 T is $\sim 0.001\%$ in our nanowire with notches, which is two to three orders of magnitude smaller than the measured MR as shown in Fig. 2(a) and (b). The negligible AMR effect is expected since the change in the spin map in our experiment is small and only exists around the notches. Compared with the 90° change across the whole sample observed from the AMR measurement, the AMR contribution in our experiment should be orders of magnitude smaller than 0.7% .

In Fig. 2(b), a significant positive Lorentz MR is observed. The Lorentz MR can be approximated as a quadratic function

of the external field B .³⁷ The red dashed lines in Fig. 2(b) show the fitted curve with eqn (4) with the coefficient $\xi = 6.5 \times 10^{-5}$,

$$\frac{\Delta\rho}{\rho} = \xi B^2 \quad (4)$$

The strength of the Lorentz MR is another indication of the crystal quality of our sample.³⁷ $\xi \approx 8 \times 10^{-4}$ has been reported in CrO₂ thin films with an RRR ratio of 71 as measured in the same longitudinal (\vec{B}/\vec{j}) configuration.⁴² In contrast, a CrO₂ sample with an RRR ratio of 11 did not show a Lorentz MR up to ~ 4 T.⁴³

Besides the AMR and Lorentz MR, we also exclude the inter-grain tunnelling magnetoresistance, which is significant in polycrystalline CrO₂,⁴⁴ because no grain boundaries are observed. Even if there are any grain boundaries, the low density of the grain boundaries contributes to negligible inter-grain tunnelling MR. The magnitude of spin disorder scattering induced by the defects and boundaries should also be small considering that the defect density in our sample is low. More importantly, both effects do not distinguish between different sample geometries, but our experiment shows that the strength of MR depends strongly on the notch geometries, which will be discussed later. Thus, we conclude that the MR effect in our measurement mainly arises from the Lorentz MR in a high field and spin curvature induced MR.

In Fig. 2(c), we decompose the overall MR *versus* B dependence into two parts. The positive part (red dashed line) is due to the strong Lorentz force on the electron motion. The negative part (blue solid line) is primarily caused by the spin curvature within the nanowire. The negative spin curvature induced MR increases linearly in a low magnetic field and becomes saturated at about ~ 3 T with a maximum MR ratio of -0.73% .

According to Levy and Zhang's model,¹⁷ the essential element inducing excess resistivity is the spatial gradient of the spin angle: $|\nabla\theta|$. $\theta(x, y)$ is the angle of a local spin relative to the x -axis. $\nabla\theta$ leads to a mixture of two spin current channels. It induces extra resistivity by partly removing the short current circuit between the two spin current channels. To capture the cumulated effect of the local spin curvature on the MR, we define the averaged spin curvature as $K = |\nabla\theta\vec{j}|_{\text{ave}}$, where $\vec{j}(x, y)$ is the unit vector of the local current density. The expression of K ensures that the spin curvature component along the local current flow direction contributes most to the excess resistivity. It is averaged over the region between the voltage leads so that the relationship between the MR and the spin curvature is retained regardless of the region we measure. For each magnetic field, the MR is derived from measurements excluding the Lorentz MR as shown in Fig. 2(c), and we calculate the spin curvature $K(B)$ based on the simulated spin map $\theta(x, y)$ in each field and the current density vector $\vec{j}(x, y)$ from COMSOL Multiphysics®.

Fig. 3(a) shows the dependence of the MR ratio on the averaged spin curvature change (relative to zero field): $\Delta K = K(B) - K(0)$ at $T = 10$ K. The star points are from the Notch-2/3 sample, measured between -0.01 T and 0.1 T. The square

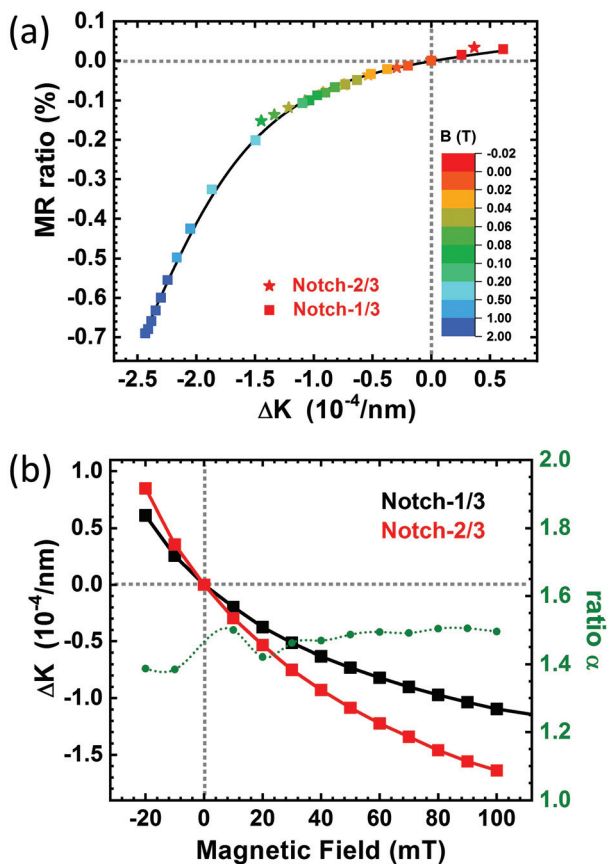


Fig. 3 (a) The relationship between the magnetoresistance and the spin curvature change (relative to zero field), $\Delta K = K(B) - K(0)$, from a simulated spin map for both the Notch-1/3 (star points) and the Notch-2/3 sample (square points). The color of the points represents the external field as shown in the color bar. The black line is the fitted curve obtained using eqn (5). (b) The calculated spin curvature change versus the external field for both the Notch-1/3 and the Notch-2/3 samples. The green line is the ratio of the spin curvature between the Notch-2/3 and the Notch-1/3 samples.

points are from the Notch-1/3 sample, measured between -0.02 T and 2 T. The fact that the square and the star points all fall on the same trendline suggests that the induced resistivity is primarily dependent on the averaged spin curvature change in a sample, and not on its detailed geometrical shape. The color of each point represents the corresponding external field applied for the MR measurement and spin curvature calculation. When $|B| < 0.1$ T, the MR ratio is almost linearly dependent on ΔK . When $|B| > 0.1$ T, the MR ratio decreases faster with ΔK , reaching the saturation point of $MR = -0.7\%$ as $K(B)$ approaches zero and ΔK approaches a minimum of $-2.5 \times 10^{-4} \text{ nm}^{-1}$. This trendline can be fitted empirically as the sum of a linear term and half of an S-shaped term (we choose tanh) centered at the saturation point,

$$\frac{\Delta\rho}{\rho} = a\Delta K + b \tanh(c(\Delta K + 2.5 \times 10^{-4} \text{ nm}^{-1})) + d \quad (5)$$

We derive parameters as follows: $a = 3.4 \text{ nm}$, $b = 6.5 \times 10^{-3}$, $c = 1 \times 10^4 \text{ nm}$, and $d = -6.5 \times 10^{-3}$.

In Fig. 3(b), we show the averaged spin curvature change, ΔK , as a function of B for both the Notch-1/3 and Notch-2/3 nanowires. As shown in Fig. 2(d)–(h), when the magnetic field is negative, the spin curvature increases ($\Delta K > 0$), and the corresponding MR is positive; when the magnetic field is positive, the spin curvature decreases ($\Delta K < 0$), and the corresponding MR is negative. The value of ΔK in Notch-2/3 is always larger than that in Notch-1/3 by a constant ratio of ~ 1.47 . This is qualitatively consistent with our measurements that in the same field, the MR ratio in Notch-2/3 is larger than that in Notch-1/3 by a factor of ~ 2.2 , and the value is 50% larger than the simulated result.

Based on our model, the excess resistivity induced by the spin curvature reported in this work shares the same physics with the domain wall resistance (DWR). We should be able to infer the DWR using eqn (5). The domain wall width in CrO_2 is estimated to be $\delta_{\text{DW}} = \pi \sqrt{\frac{A}{K_{\text{u}}}} = 70.2 \text{ nm}$.^{34,45} Assuming that the angle of the spin changes with the position x as the function $\cos \theta = \tanh\left(\frac{\pi x}{\delta_{\text{DW}}}\right)$,^{36,45,46} the averaged spin curvature in the range of $(-35, 35) \text{ nm}$ is $3.3 \times 10^{-2} \text{ nm}^{-1}$, which corresponds to a DWR of 19% based on eqn (5). This value is a bit larger than that mentioned in a previous report on the DWR of CrO_2 , which estimated that $\frac{\Delta\rho_{\text{DW}}}{\rho}$ is in the range of 1.3% to 13% at 5.0 K.³⁶ This discrepancy arises from the assumption of $\cos \theta = \tanh\left(\frac{\pi x}{\delta_{\text{DW}}}\right)$: the spin curvature is only along the x -axis and ignores the y -axis direction. Alternatively, we have simulated a domain wall in CrO_2 with the parameters mentioned before and obtained the spin curvature $K = 4.7 \times 10^{-3} \text{ nm}^{-1}$ when the current flows perpendicular to the DW. The domain wall resistivity is estimated to be $\sim 3\%$, which is consistent with the published DWR range of 1.3% to 13%.³⁶ The DWR of 3% implies a high spin asymmetry of $\frac{\rho_{\uparrow}}{\rho_{\downarrow}} \approx 2000$ based on the model of Levy and Zhang.¹⁷

Finally, we present the change of the magnetoresistance with temperature. As shown in Fig. 4(a), the MR ratio changes linearly with the external field. The slope of the MR ratio versus the magnetic field decreases from 10 K to 200 K. By fitting the linear relationship between the MR ratio and B , we obtained the slope $\frac{\Delta MR}{\Delta B}$ within temperature ranges from 10 K to 250 K as shown in Fig. 4(b). It shows that the magnitude of the slope $\frac{\Delta MR}{\Delta B}$ decreases with increasing temperature for both Notch-1/3 and Notch-2/3 nanowires. It is primarily because half-metallicity is a low temperature physics phenomenon.⁴⁷ At higher temperatures, the increasing magnon population causes increasing density of states at the Fermi surface for the minority spins. The reduced spin asymmetry lessens the effect of the spin curvature in generating excess resistivity.

From 10 K to 200 K, the slope of Notch-2/3 is always larger than that of Notch-1/3 due to the larger spin curvature. At

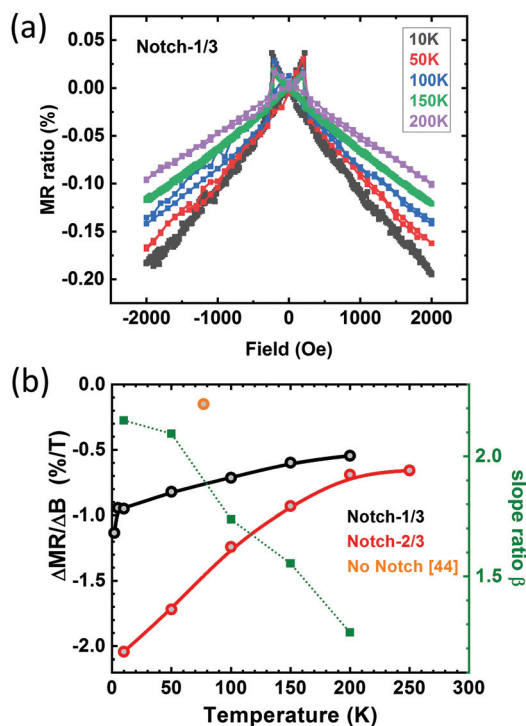


Fig. 4 (a) Magnetoresistance of the Notch-1/3 sample at 10 K to 200 K in the field range of -0.2 T to 0.2 T. (b) The slope $\frac{\Delta\text{MR}}{\Delta B}$ versus temperature for the Notch-1/3 sample (black dots), the Notch-2/3 sample (red dots), and the sample with no notch (orange dot) from ref. 44. The green line represents the ratio of $\frac{\Delta\text{MR}}{\Delta B}$ between the Notch-2/3 and Notch-1/3 samples.

10 K, the slope is $\frac{\Delta\text{MR}}{\Delta B} = -0.95\%/T$ for Notch-1/3 and $-2.0\%/T$ for Notch-2/3. At 100 K, $\frac{\Delta\text{MR}}{\Delta B}$ is $-1.2\%/T$ for Notch-2/3 and -0.7% for Notch-1/3. For comparison, we include the data point for an epitaxial CrO_2 nanowire without notches, showing that at 77 K the slope $\frac{\Delta\text{MR}}{\Delta B}$ is $-0.15\%/T$,⁴⁴ which is about one order of magnitude smaller than those of our nanowires with the notches due to their negligible spin curvature. It further confirms that by introducing notches into the nanowires, the induced spin curvature generates excess resistivity effectively. The ratio of the slope $\frac{\Delta\text{MR}}{\Delta B}$ between Notch-2/3 and Notch-1/3 samples is represented by the green curve in Fig. 4(b). The slope ratio is at its largest at 2.2 at 10 K, primarily because the spin curvature of the Notch-2/3 sample doubles that of the Notch-1/3 sample. As the temperature is increased, the slope ratio decreases steadily, decreasing to 1.3 at 200 K. The decrease of the slope also proves the decrease of the spin curvature induced resistivity, which depends highly on the sample geometry. At higher temperatures, other mechanisms such as the suppression of spin fluctuation by the magnetic field may contribute to the MR.^{48,49} Therefore, the curves of $\frac{\Delta\text{MR}}{\Delta B}$ for

Notch-1/3 and Notch-2/3 converge at high temperatures, and the ratio of the slope decreases to ward 1.0.

Conclusion

We have quantitatively measured spin curvature induced resistivity in epitaxial half-metallic CrO_2 nanowires. The spin curvature is introduced by creating notches along the edge of the nanowires. An external magnetic field is used to control the degree of spin curvature and to observe magnetoresistance. Our analysis shows a strong dependence of magnetoresistance on the spin curvature. This relationship of resistivity *versus* spin curvature is linear when the magnetic field is in the range of ± 0.1 T. MR measurements at different temperatures show that the effect of spin curvature on the resistivity is the highest at low temperature. It offers insight into the influence of the thermal effect on half-metallicity, which is highly relevant to spintronics application using half-metals at room temperature. We have estimated the magnetic domain wall resistivity for CrO_2 based on our obtained relationship between spin curvature and induced resistivity and concluded that it is consistent with the experimentally measured value of DWR.

Conflicts of interest

There are no conflicts to declare.

Acknowledgements

The work was supported by the King Abdullah University of Science and Technology (KAUST) under the Sensor Initiative.

References

- 1 N. Nagaosa, J. Sinova, S. Onoda, A. H. MacDonald and N. P. Ong, *Rev. Mod. Phys.*, 2010, **82**, 1539.
- 2 Q. Hao, W. Chen, S. Wang and G. Xiao, *J. Appl. Phys.*, 2017, **122**, 033901.
- 3 J. Hirsch, *Phys. Rev. Lett.*, 1999, **83**, 1834.
- 4 J. Sinova, S. O. Valenzuela, J. Wunderlich, C. Back and T. Jungwirth, *Rev. Mod. Phys.*, 2015, **87**, 1213.
- 5 L. Liu, C.-F. Pai, Y. Li, H. W. Tseng, D. C. Ralph and R. A. Buhrman, *Science*, 2012, **336**, 555–558.
- 6 I. M. Miron, K. Garello, G. Gaudin, P.-J. Zermatten, M. V. Costache, S. Auffret, S. Bandiera, B. Rodmacq, A. Schuhl and P. Gambardella, *Nature*, 2011, **476**, 189.
- 7 W. Chen, L. Qian and G. Xiao, *Sci. Rep.*, 2018, **8**, 8144.
- 8 W. Chen, G. Xiao, Q. Zhang and X. Zhang, *Phys. Rev. B: Condens. Matter Mater. Phys.*, 2018, **98**, 134411.
- 9 L. Qian, W. Chen, K. Wang, X. Wu and G. Xiao, *AIP Adv.*, 2018, **8**, 115323.
- 10 S. S. Parkin, M. Hayashi and L. Thomas, *Science*, 2008, **320**, 190–194.

- 11 W. Chen, L. Qian and G. Xiao, *AIP Adv.*, 2018, **8**, 055918.
- 12 J. F. Gregg, W. Allen, K. Ounadjela, M. Viret, M. Hehn, S. M. Thompson and J. M. D. Coey, *Phys. Rev. Lett.*, 1996, **77**, 1580–1583.
- 13 U. Ebels, A. Radulescu, Y. Henry, L. Piraux and K. Ounadjela, *Phys. Rev. Lett.*, 2000, **84**, 983.
- 14 A. D. Kent, J. Yu, U. Rüdiger and S. S. Parkin, *J. Phys.: Condens. Matter*, 2001, **13**, R461.
- 15 T. McGuire and R. Potter, *IEEE Trans. Magn.*, 1975, **11**, 1018–1038.
- 16 M. N. Baibich, J. M. Broto, A. Fert, F. N. Van Dau, F. Petroff, P. Etienne, G. Creuzet, A. Friederich and J. Chazelas, *Phys. Rev. Lett.*, 1988, **61**, 2472.
- 17 P. M. Levy and S. Zhang, *Phys. Rev. Lett.*, 1997, **79**, 5110.
- 18 I. Campbell and A. Fert, *Handbook of Ferromagnetic Materials*, 1982, vol. 3, pp. 747–804.
- 19 V. Musle, A. Kumar and S. Choudhary, *J. Alloys Compd.*, 2019, **770**, 345–349.
- 20 N. Pandey, A. Kumar and S. Chakrabarti, *ACS Appl. Mater. Interfaces*, 2019, **11**, 39248–39253.
- 21 N. Pandey, A. Kumar and S. Chakrabarti, *RSC Adv.*, 2019, **9**, 29556–29565.
- 22 N. Pandey, A. Kumar and S. Chakrabarti, *Appl. Surf. Sci.*, 2020, **504**, 144411.
- 23 K. Wang, L. Qian, W. Chen, S.-C. Ying, G. Xiao and X. Wu, *Phys. Rev. B: Condens. Matter Mater. Phys.*, 2019, **99**, 184410.
- 24 K. Wang, L. Qian, S.-C. Ying, G. Xiao and X. Wu, *Nanoscale*, 2019, **11**, 6952–6961.
- 25 D. A. Allwood, G. Xiong, C. Faulkner, D. Atkinson, D. Petit and R. Cowburn, *Science*, 2005, **309**, 1688–1692.
- 26 A. Kumar and S. Choudhary, *J. Supercond. Novel Magn.*, 2018, **31**, 3245–3250.
- 27 N. Pandey, A. Kumar and S. Chakrabarti, *J. Magn. Magn. Mater.*, 2019, 166073.
- 28 K. Schwarz, *J. Phys. F: Met. Phys.*, 1986, **16**, L211.
- 29 Y. Ji, G. J. Strijkers, F. Y. Yang, C. L. Chien, J. M. Byers, A. Anguelouch, G. Xiao and A. Gupta, *Phys. Rev. Lett.*, 2001, **86**, 5585–5588.
- 30 R. Soulen, J. Byers, M. Osofsky, B. Nadgorny, T. Ambrose, S. Cheng, P. R. Broussard, C. Tanaka, J. Nowak and J. Moodera, *Science*, 1998, **282**, 85–88.
- 31 K. P. Kamper, W. p. Schmitt, G. Guntherodt, R. J. Gambino and R. Ruf, *Phys. Rev. Lett.*, 1987, **59**, 2788–2791.
- 32 S. P. Lewis, P. B. Allen and T. Sasaki, *Phys. Rev. B: Condens. Matter Mater. Phys.*, 1997, **55**, 10253.
- 33 L. Chioncel, H. Allmaier, E. Arrigoni, A. Yamasaki, M. Daghofer, M. Katsnelson and A. Lichtenstein, *Phys. Rev. B: Condens. Matter Mater. Phys.*, 2007, **75**, 140406.
- 34 G. Miao, G. Xiao and A. Gupta, *Phys. Rev. B: Condens. Matter Mater. Phys.*, 2005, **71**, 094418.
- 35 X. Zou and G. Xiao, *Appl. Phys. Lett.*, 2007, **91**, 113512.
- 36 W. Chen, L. Qian and G. Xiao, *Phys. Rev. B: Condens. Matter Mater. Phys.*, 2018, **98**, 174402.
- 37 M. Rabe, J. Pommer, K. Sann, B. Özyilmaz, C. König, M. Fraune, U. Rüdiger, G. Güntherodt, S. Senz and D. Hesse, *J. Phys.: Condens. Matter*, 2001, **14**, 7.
- 38 A. Vansteenkiste, J. Leliaert, M. Dvornik, M. Helsen, F. Garcia-Sanchez and B. Van Waeyenberge, *AIP Adv.*, 2014, **4**, 107133.
- 39 J. Leliaert, J. Mulkers, J. De Clercq, A. Coene, M. Dvornik and B. Van Waeyenberge, *AIP Adv.*, 2017, **7**, 125010.
- 40 W. Thomson, *Proc. R. Soc. London*, 1857, **8**, 546–550.
- 41 M. Anwar and J. Aarts, *Phys. Rev. B: Condens. Matter Mater. Phys.*, 2013, **88**, 085123.
- 42 S. M. Watts, S. Wirth, S. Von Molnar, A. Barry and J. Coey, *Phys. Rev. B: Condens. Matter Mater. Phys.*, 2000, **61**, 9621.
- 43 K. Suzuki and P. Tedrow, *Phys. Rev. B: Condens. Matter Mater. Phys.*, 1998, **58**, 11597.
- 44 X. Zou and G. Xiao, *Phys. Rev. B: Condens. Matter Mater. Phys.*, 2008, **77**, 054417.
- 45 D. Chiba, M. Yamanouchi, F. Matsukura, T. Dietl and H. Ohno, *Phys. Rev. Lett.*, 2006, **96**, 096602.
- 46 A. Brataas, G. Tatara and G. E. Bauer, *Phys. Rev. B: Condens. Matter Mater. Phys.: Condens. Matter Mater. Phys.*, 1999, **60**, 3406.
- 47 H. Fujiwara, K. Terashima, M. Sunagawa, Y. Yano, T. Nagayama, T. Fukura, F. Yoshii, Y. Matsuura, M. Ogata and T. Wakita, *Phys. Rev. Lett.*, 2018, **121**, 257201.
- 48 K. Ueda, *Solid State Commun.*, 1976, **19**, 965–968.
- 49 H. Yamada and S. Takada, *J. Phys. Soc. Jpn.*, 1973, **34**, 51–57.